Partition function zeros of a restricted Potts model on lattice strips and effects of boundary conditions

2006 J. Phys. A: Math. Gen. 39 10277

(http://iopscience.iop.org/0305-4470/39/33/002)

INSTITUTE OF PHYSICS PUBLISHING JOURNAL OF PHYSICS A: MATHEMATICAL AND GENERAL

J. Phys. A: Math. Gen. **39** (2006) 10277–10295 doi:10.1088/0305-4470/39/33/002

Partition function zeros of a restricted Potts model on lattice strips and effects of boundary conditions

Shu-Chiuan Chang[1] **and Robert Shrock**[2]

[1] Department of Physics, National Cheng Kung University, Tainan 70101, Taiwan
[2] C N Yang Institute for Theoretical Physics, State University of New York, Stony Brook, NY 11794, USA

Received 2 March 2006, in final form 6 June 2006
Published 2 August 2006
Online at stacks.iop.org/JPhysA/39/10277

Abstract

We calculate exactly the partition function $Z(G, Q, v)$ of the Q-state Potts model with temperature-like Boltzmann variable v for strip graphs G of the square and triangular lattices of various widths L_y and arbitrarily great lengths L_x, with a variety of boundary conditions, and with Q and v restricted to satisfy conditions corresponding to the ferromagnetic phase transition on the associated two-dimensional lattices. From these calculations, in the limit $L_x \to \infty$, we determine the continuous accumulation loci $\mathcal{B}$ of the partition function zeros in the v and Q planes. Strips of the honeycomb lattice are also considered. We discuss some general features of these loci.

PACS numbers: 05.20.−y, 64.60.Cn, 75.10.Hk

1. Introduction

The Q-state Potts model has served as a valuable model for the study of phase transitions and critical phenomena [1–3]. In this paper we study the zeros of the Q-state Potts model partition function on lattice strip graphs of fixed width L_y and arbitrarily great length L_x, with Q and the temperature-like variable v restricted to satisfy the condition for the ferromagnetic phase transition on the associated two-dimensional lattice. From these calculations, in the limit $L_x \to \infty$, we exactly determine the continuous accumulation loci $\mathcal{B}$ of the partition function zeros in the v and Q planes.

We begin by briefly recalling the definition of the model and some relevant notation. On a graph G at temperature T, the Potts model is defined by the partition function:

$$Z(G, Q, v) = \sum_{\{\sigma\}} \exp\left(K \sum_{\langle ij \rangle} \delta_{\sigma_i \sigma_j} \right), \tag{1}$$

where $\sigma_i = 1, \ldots, Q$ are the classical spin variables on each vertex (site) $i \in G$, $\langle ij \rangle$ denotes pairs of adjacent vertices, $K = \beta J$ where $\beta = (k_B T)^{-1}$ and J is the spin–spin coupling.

We define $v = e^K - 1$, so that v has the physical range of values $0 \leqslant v \leqslant \infty$ and $-1 \leqslant v \leqslant 0$ for the respective ferromagnetic and antiferromagnetic cases $J > 0$ and $J < 0$. The graph $G = G(V, E)$ is defined by its vertex set V and its edge (bond) set E. The number of vertices of G is denoted as $n = n(G) = |V|$ and the number of edges of G as $e(G) = |E|$. The Potts model can be generalized from non-negative integer Q and physical v to real and, indeed, complex Q and v via the cluster relation [16, 17] $Z(G, Q, v) = \sum_{G' \subseteq G} Q^{k(G')} v^{e(G')}$, where $G' = (V, E')$ with $E' \subseteq E$, and $k(G')$ denotes the number of connected components of G'.

Although the infinite-length, finite-width strips that we consider here are quasi-one-dimensional systems and the free energy is analytic for all nonzero temperatures, it is nevertheless of interest to investigate the properties of the Potts model with the variables Q and v restricted to satisfy the above conditions. There are several reasons for this. First, for an $L_y \times L_x$ section of the respective type of lattice, as $L_x \to \infty$ and $L_y \to \infty$ with L_y/L_x equal to a finite nonzero constant, one sees the onset of two-dimensional critical behaviour. Thus, the strips with $L_x \to \infty$ and L_y fixed provide a type of interpolation between the one-dimensional line and the usual two-dimensional thermodynamic limit as L_y increases. Second, one can obtain exact results for the partition function $Z(G, Q, v)$ and (reduced) free energy $f = \lim_{n\to\infty} n^{-1} \ln Z$. The value of such exact results is clear since it has not so far been possible to solve exactly for $f(\Lambda, Q, v)$ for arbitrary Q and v on a lattice Λ with dimensionality $d \geqslant 2$, and the only exact solution for arbitrary v is for the $d = 2$ Ising case $Q = 2$. Hence, exact results on the model for infinite-length, finite-width strips complement the standard set of approximate methods that are used for $d \geqslant 2$, such as series expansions and Monte Carlo simulations. Although the singular locus $\mathcal{B}_v$ does not intersect the real axis on the physical finite-temperature interval $-1 < v < \infty$ for the infinite-length, finite-width strips under consideration here, properties of the corresponding locus $\mathcal{B}_Q$, can give insight into the corresponding locus $\mathcal{B}_Q$ for the respective two-dimensional lattices. This type of connection was shown to hold in our earlier studies, which focused on the singular locus $\mathcal{B}$ of the Potts model free energy in the v plane for fixed Q or in the Q plane for fixed v. For example, in [4] and [5] we obtained exact solutions for $Z(G, Q, v)$ for arbitrary Q and v on strips of the square lattice with widths $L_y = 2$ and $L_y = 3$, respectively, and from these solutions we determined the corresponding loci $\mathcal{B}$ in the limit of infinite length. It was shown in [4] and [5] that for the Ising case $Q = 2$, on these strips with periodic longitudinal boundary conditions, the loci $\mathcal{B}_v$ contain the points $v = -1 \pm i$ (as multiple points in the sense of algebraic geometry). This property is the same as is true of the analogous locus for the Ising model on the (infinite) square lattice, which is the union of the circles $|v| = \sqrt{2}$ and $|v + 2| = \sqrt{2}$ [6]. Similarly, in [7] and [8] we showed that the corresponding loci $\mathcal{B}_v$ for infinite-length strips of the triangular and honeycomb lattices with width $L_y = 2$ again contain these points $v = -1 \pm i$ (as multiple points), the same as is true of the analogous loci for the Ising model on the triangular and honeycomb lattices [9, 10].

These correspondences were also evident for the locus $\mathcal{B}_Q$ for fixed v. For example, consider the special case $v = -1$ where the Potts model partition function is equal to the chromatic polynomial counting the number of ways of assigning Q colours to the vertices of a graph, subject to the constraint that no adjacent vertices have the same colour. The ground state degeneracy per site, $W(\{G\}, Q) = \lim_{n\to\infty} Z(G, Q, -1)^{1/n}$ (where $\{G\}$ denotes the formal limit of the graph G as $n \to \infty$), has a different analytic behaviour for $Q > Q_c$ and $Q < Q_c$, where the critical value, Q_c, is the maximal point where $\mathcal{B}_Q$ crosses the positive real axis [11]. Using new exact solutions for $W(\{G\}, Q)$, we showed in [12] that for cyclic self-dual strips of the square lattice, $Q_c = 3$, exactly the same as the value for the infinite square lattice [13]. This was also true for the $L_y = 3$ strip of the square lattice with toroidal or Klein bottle boundary conditions [14]. As these examples show, the properties of the singular loci $\mathcal{B}_v$

for fixed Q and $\mathcal{B}_Q$ of the Potts model free energy for fixed v calculated for infinite-length, finite-width strips can exhibit certain properties in common with the analogous loci on the corresponding (infinite) two-dimensional lattices. Indeed, one of the interesting results of the present work is the key role of the point $Q = 4$ for the locus $\mathcal{B}_Q$, which makes a connection with the locus $\mathcal{B}_Q$ for the physical phase transition of the Potts model on two-dimensional lattices. We recall that the ferromagnetic phase transition of the 2D Potts model is continuous (second order) for $0 \leqslant Q \leqslant 4$ and first order for $Q > 4$.

The above-mentioned loci are determined by the equality in magnitude of the eigenvalues of the transfer matrix of the model with maximal modulus and hence are also called the set of equimodular curves (where 'curve' is used in a general sense that also includes line segments). A similar study has been carried out for a special set of strips of the square lattice, namely those with an exact self-duality property [15]. It is of considerable interest to investigate which features of the loci of zeros found in that special case depend on the self-duality and which are more general. Here we study and answer this question using strips of the square, triangular and honeycomb lattices with a variety of different boundary conditions.

The Potts model partition function is equivalent to an important function in mathematical graph theory, the Tutte polynomial $T(G, x, y)$ [18–21]:

$$Z(G, Q, v) = (x-1)^{k(G)}(y-1)^{n(G)}T(G, x, y), \tag{2}$$

where

$$x = 1 + \frac{Q}{v}, \qquad y = 1 + v. \tag{3}$$

The phase transition temperatures of the ferromagnetic Potts model (in the thermodynamic limit) on the square (sq), triangular (t) and honeycomb (hc) lattices are given, respectively, by the physical solutions to the equations [1]

$$Q = v^2 \quad \text{(sq)} \tag{4}$$

$$Q = v^2(v+3) \quad \text{(t)} \tag{5}$$

and

$$Q^2 + 3Qv - v^3 = 0 \quad \text{(hc)}. \tag{6}$$

Conditions (5) and (6) are equivalent, owing to the duality of the triangular and honeycomb lattices. In terms of the Tutte variables, these conditions are $(y-1)(x-y) = 0$ for $\Lambda = \text{sq}$, $(y-1)(y^2+y-x-1) = 0$ for $\Lambda = t$ and $(y-1)^2(x^2+x-y-1) = 0$ for $\Lambda = \text{hc}$. Since $y = 1$ means $K = 0$, i.e., infinite temperature, the root at $y = 1$ is not relevant; dividing both sides of these three equations by the appropriate powers of $(y-1)$, we thus obtain the conditions $x = y$ (sq), $y^2 + y - x - 1 = 0$ (t) and $x^2 + x - y - 1 = 0$ (hc).

We next describe the boundary conditions that we consider. The longitudinal and transverse directions of the lattice strip are taken to be horizontal (in the x direction) and vertical (in the y direction). The boundary conditions that are free, periodic and periodic with reversed orientation of sites on the transverse boundary slice are labelled as F, P and TP (where T stands for 'twisted'). We consider strips with the following types of boundary conditions:

(i) (FBC_y, FBC_x) = free
(ii) (FBC_y, PBC_x) = cyclic (cyc)
(iii) $(FBC_y, TPBC_x)$ = Möbius (Mb)
(iv) (PBC_y, FBC_x) = cylindrical (cyl)

(v) (PBC_y, PBC_x) = toroidal (tor)
(vi) $(PBC_y, TPBC_x)$ = Klein bottle (Kb).

We thus denote a strip graph of a given type of lattice Λ = sq or t as $\Lambda[L_y \times L_x]$, BC, where BC = free for (FBC_y, FBC_x) and similarly for the other boundary conditions. In earlier work we showed that although the partition functions $Z(\Lambda[L_y \times L_x], BC, Q, v)$ are different for cyclic and Möbius boundary conditions, $\mathcal{B}$ is the same for these two, and separately that although this partition function is different for toroidal and Klein-bottle boundary conditions, $\mathcal{B}$ is the same for these two latter conditions [4], [5–8]. Therefore, we shall focus here on the cases of free, cyclic, cylindrical and toroidal boundary conditions.

Our procedure for calculating $Z(G, Q, v)$ on these strips is as follows. For the square and triangular lattices, equations (4) and (5) have the simplifying feature that they have the form $Q = g_\Lambda(v)$, where $g_\Lambda(v)$ is a polynomial in v. Accordingly, to restrict Q and v to satisfy the phase transition conditions for the respective two-dimensional lattices, we start with the exact partition function and replace Q by $g_\Lambda(v)$ for Λ = sq and $\Lambda = t$. We then solve for the zeros of $Z(G, g_\Lambda(v), v)$ and, in the $L_x \to \infty$ limit, the continuous accumulation loci $\mathcal{B}_v$ in the complex v plane. The image of these zeros and loci under the respective mappings (4) and (5) yield the zeros and loci in the complex Q plane. In the case of the honeycomb (hc) lattice, the ferromagnetic phase transition condition (6) is nonlinear in both v and Q. Since it is of lower degree in Q, we solve for this variable, obtaining $Q = (v/2)(-3 \pm \sqrt{9+4v})$. Of course, only one of these solutions is physical for the actual two-dimensional lattice, namely the one with the plus sign. Given the fact that the triangular and honeycomb lattices are dual to each other and the consequence that properties of the phase transition of the ferromagnetic Potts model on the triangular lattice are simply related to those on the honeycomb lattice, it follows that, insofar as we are interested in applying our exact results on infinite-length, finite-width strips to two dimensions, it suffices to concentrate on strips of either the triangular or honeycomb lattice. Since condition (5) is easier to implement than the solution for Q on the honeycomb lattice, we shall mainly focus on strips of the triangular lattice, but also include some comments on honeycomb-lattice strips.

We denote the Tutte–Beraha numbers [19–23]:

$$Q_r = 4\cos^2(\pi/r). \tag{7}$$

For the range of interest here, $1 \leqslant r \leqslant \infty$, we note that Q_r monotonically decreases from 4 to 0 as r increases from 1 to 2, and then Q_r increases monotonically from 0 to 4 as r increases from 2 to ∞. For our analysis of strips of the square lattice, it will also be useful to denote $v_r = -2\cos(\pi/r)$ so that $Q_r = v_r^2$. Further background is given in [15].

2. Some general structural properties

For these strips, the partition function has the general form (with $L_x = m$)

$$Z(\Lambda[L_y \times m], BC, Q, v) = \sum_j c_j (\lambda_{\Lambda,BC,L_y,j})^m, \tag{8}$$

where the coefficients c_j are independent of m. It will be convenient to separate out a power of v and write

$$\lambda_{\Lambda,BC,L_y,j} = v^{L_y}\bar{\lambda}_{\Lambda,BC,L_y,j}. \tag{9}$$

We denote cyclic strips of the lattice Λ of width L_y and length $L_x \equiv m$ as $\Lambda[L_y \times m]$, cyc. The partition function has the general form [24–26]

$$Z(\Lambda[L_y \times m], \mathrm{cyc}, Q, v) = \sum_{d=0}^{L_y} c^{(d)} \sum_{j=1}^{n_Z(L_y,d)} (\lambda_{\Lambda,L_y,d,j})^m, \tag{10}$$

where we use simplified notation by setting $\lambda_{\Lambda,\mathrm{cyc},L_y,d,j} \equiv \lambda_{\Lambda,L_y,d,j}$ and $\bar{\lambda}_{\Lambda,\mathrm{cyc},L_y,d,j} \equiv \bar{\lambda}_{\Lambda,L_y,d,j}$, and where

$$n_Z(L_y,d) = \frac{(2d+1)}{(L_y+d+1)}\binom{2L_y}{L_y-d} \tag{11}$$

for $0 \leqslant d \leqslant L_y$ and zero otherwise, and

$$c^{(d)} = \sum_{j=0}^{d}(-1)^j\binom{2d-j}{j}Q^{d-j}. \tag{12}$$

The first few of these coefficients are $c^{(0)} = 1$, $c^{(1)} = Q-1$, $c^{(2)} = Q^2-3Q+1$ and $c^{(3)} = Q^3-5Q^2+6Q-1$. The form (10) applies for cyclic strips of not just the square lattice, but also the triangular and honeycomb lattices [8, 26]. The total number of eigenvalues is

$$N_{Z,L_y,\lambda} = \sum_{d=0}^{L_y} n_Z(L_y,d) = \binom{2L_y}{L_y}. \tag{13}$$

Since $n_Z(L_y,L_y) = 1$, i.e., there is only a single $\lambda_{\Lambda,L_y,d,j}$ for $d = L_y$, we denote it simply as $\lambda_{\Lambda,L_y,L_y}$. The single reduced eigenvalue with $d = L_y$ is

$$\bar{\lambda}_{\Lambda,L_y,L_y} = 1. \tag{14}$$

We now proceed with our results. We shall point out relevant features for the widths that we consider; of course, it is possible to study larger widths, but, as our discussion will show, relevant features are already present for the widths that we consider.

3. Strips of the square lattice

3.1. Free strips

We denote these strips as sq$[L_y \times m]$, free. For $L_y = 1$, an elementary calculation yields $Z = Q(Q+v)^{m-1}$. Setting $Q = v^2$ yields

$$Z(\mathrm{sq}[1\times m],\mathrm{free},v^2,v) = v^{m+1}(v+1)^{m-1}, \tag{15}$$

which has zeros only at the two discrete points $v = 0$ and $v = -1$. In this case the continuous $\mathcal{B}$ degenerates to these two points.

For $L_y = 2$, we use the partition function $Z(\mathrm{sq}[2\times m],\mathrm{free},Q,v)$, calculated in [4], which has the form (8) with two λs. For $Q = v^2$, we find

$$\bar{\lambda}_{\mathrm{sq},2,0,j} = \tfrac{1}{2}[(v+2)^2 \pm (v^4+4v^3+12v^2+20v+12)^{1/2}], \tag{16}$$

where $j = 1, 2$ correspond to $\pm$. In the infinite-length limit, the continuous accumulation set of loci $\mathcal{B}_v$ and, correspondingly, $\mathcal{B}_Q$ are shown in figures 1 and 2. They consist of two complex-conjugate arcs that intersect each other and cross the real v axis at $v = -2$ and equivalently, the real Q axis at $Q = 4$. The endpoint of these arcs in the v plane occurs at the roots of the polynomial in the square root of $\bar{\lambda}_{\mathrm{sq},2,0,j}$, namely $v = -1.33 \pm 0.23\mathrm{i}$ and $-0.67 \pm 2.48\mathrm{i}$, and hence $Q = 1.71 \pm 0.61\mathrm{i}$ and $Q = -5.71 \pm 3.34\mathrm{i}$. For comparison, in this and other figures we show zeros of the partition function for long finite strips; in this case, $m = 40$. One sees that the zeros lie rather close to the asymptotic loci $\mathcal{B}$ and that the density of zeros increases as one approaches the endpoints of the arcs.

In these figures and others shown below, there are also zeros of the partition function that do not lie on the asymptotic accumulation loci. For example, in general, for any graph G, the cluster relation given above shows that $Z(G,Q,v) = 0$ at the point $(Q,v) = (0,0)$,

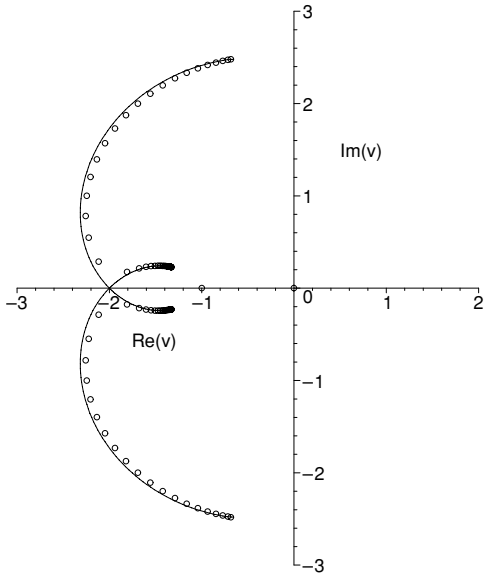

Figure 1. Locus $\mathcal{B}_v$ for the Potts model on a $2 \times \infty$ strip of the square lattice with free boundary conditions and with Q and v satisfying (4). Partition function zeros are shown for a 2×40 strip.

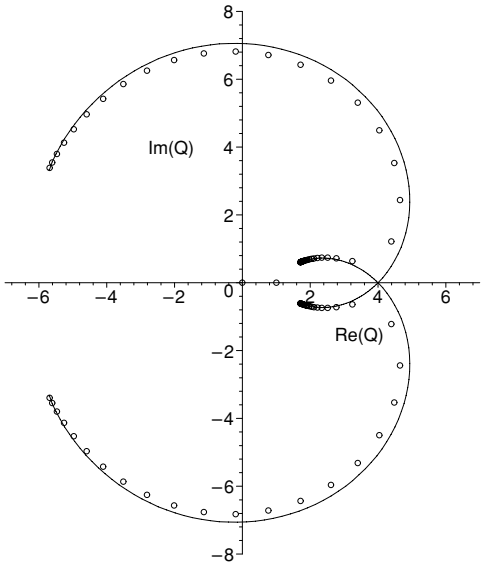

Figure 2. Locus $\mathcal{B}_Q$ for the Potts model on a $2 \times \infty$ strip of the square lattice with free boundary conditions and with Q and v satisfying (4). Partition function zeros are shown for a 2×40 strip.

which lies on manifolds defined by all of equations (4)–(6). Depending on the type of lattice strip graph, this may or may not be an isolated zero or lie on the continuous accumulation set of zeros, $\mathcal{B}$. For example, for the $L_y = 2$ square-lattice strips with free or cylindrical boundary conditions it is isolated (cf figures 1–3), while for the $L_y = 2$ strips with cyclic or toroidal boundary conditions, it lies on the loci $\mathcal{B}$ in the v and Q planes (cf figures 4–6) and

similarly for the triangular strips to be discussed below. Another general result is that for a graph G with at least one edge, $Z(G, Q, v) = 0$ at the point $(Q, v) = (1, -1)$. This follows because $Z(G, Q, -1)$, the partition function for the zero-temperature Potts antiferromagnet, is precisely the chromatic polynomial $P(G, Q)$, which counts the number of ways one can assign colours from a set of Q colours to the vertices of G, subject to the condition that no two adjacent vertices have the same colour. These are called proper colourings of G. Clearly, the number of these proper colourings of a graph G vanishes if it has at least one edge and there is only one colour, i.e., if $Q = 1$. This point $(Q, v) = (1, -1)$ is on the manifold defined by (4) for the square lattice (although not on the corresponding manifolds defined by equations (5) and (6) for the triangular and honeycomb lattices). Thus, one sees a zero at this point in the plots for the square-lattice strips. In the cases we have studied, this zero is isolated.

For $L_y = 3$, we use the exact calculation of $Z(\mathrm{sq}[3 \times m], \mathrm{free}, Q, v)$ for general Q and v in [5] and specialize to $Q = v^2$. The partition function depends on (mth powers of) four eigenvalues which are roots of a quartic equation ((A.8) in [5]). In the limit $L_x \to \infty$, $\mathcal{B}_v$ consists of complex-conjugate pairs of arcs, all of which pass through the point $v = -2$, where all four roots of the above quartic equation are degenerate in magnitude. The arcs lying farthest from the real axis cross the imaginary v axis (at $v \simeq \pm 2.96\mathrm{i}$). Hence, the image of this locus under the map $Q = v^2$ in the Q plane, $\mathcal{B}_Q$, also consists of complex-conjugate arcs which all pass through the point $Q = 4$. Furthermore, two of these cross the negative real Q axis, so that $\mathcal{B}_Q$ separates the Q plane into regions. There are also other zeros on the negative real v axis, and hence resultant zeros on the positive real Q axis. Using the calculations of $Z(\mathrm{sq}[L_y \times m], \mathrm{free}, Q, v)$ in [27, 28], we have performed the corresponding analyses for $L_y = 4, 5$ and found similar features.

3.2. Cylindrical strip

We find that $Z(\mathrm{sq}[2 \times m], \mathrm{cyl}, v^2, v)$ has the form (8) depending on two $\bar{\lambda}$s, which are

$$\bar{\lambda}_{\mathrm{sqcyl},j} = \tfrac{1}{2}\left[3v^2 + 8v + 6 \pm (v+2)\sqrt{5v^2 + 12v + 8}\right], \tag{17}$$

where $j = 1, 2$ correspond to $\pm$ and sqcyl refers to this type of strip. In the limit $m \to \infty$, the locus $\mathcal{B}_v$ consists of a self-conjugate arc that crosses the real axis at $v = -2$ and has endpoints at the roots of the polynomial in the square root in (17), namely, $v = (-6 \pm 2\mathrm{i})/5$. Thus, $\mathcal{B}_Q$ consists of an arc that crosses the real axis at $Q = 4$ and has endpoints at $Q = (32 \pm 24\mathrm{i})/25$. The locus $\mathcal{B}_Q$ and partition function zeros for a long finite strip are shown in figure 3. As was the case with the free strips, the density of zeros increases as one approaches the endpoints of the arcs.

3.3. Cyclic and Möbius strips

For $L_y = 1$, $\mathrm{sq}[1 \times m]$ is just the circuit graph with m vertices, C_m. An elementary calculation yields $Z(C_m, Q, v) = (Q + v)^m + c^{(1)}v^m$, so for $Q = v^2$, one has $\bar{\lambda}_{\mathrm{sq},1,0} = v + 1$ and $\bar{\lambda}_{\mathrm{sq},1,1} = 1$ as in (14), and

$$Z(C_m, v^2, v) = v^m(v+1)[(v+1)^{m-1} + v - 1]. \tag{18}$$

The resultant locus $\mathcal{B}_v$ is the circle $|v + 1| = 1$, i.e.,

$$v = -1 + \mathrm{e}^{\mathrm{i}\phi}, \qquad 0 \leqslant \phi \leqslant 2\pi, \tag{19}$$

which crosses the real v axis at $v = 0$ and $v = -2$. The resultant locus $\mathcal{B}_Q$ with $Q = v^2$ is given by

$$\mathrm{Re}(Q) = 2\cos\phi(\cos\phi - 1), \qquad \mathrm{Im}(Q) = 2\sin\phi(\cos\phi - 1) \tag{20}$$

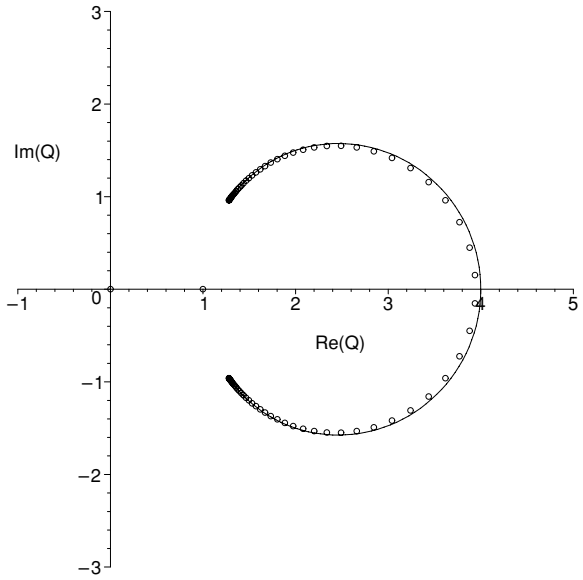

Figure 3. Locus $\mathcal{B}_Q$ for the Potts model on a $2 \times \infty$ strip of the square lattice with cylindrical boundary conditions and with Q and v satisfying (4). Partition function zeros are shown for a cylindrical 2×40 strip.

for $0 \leqslant \phi \leqslant 2\pi$. This locus crosses the real Q axis at $Q = Q_2 = 0$, where it has a cusp, and at $Q = Q_1 = Q_\infty = 4$; it also crosses the imaginary Q axis at $Q = \pm 2\mathrm{i}$. The loci $\mathcal{B}_v$ and $\mathcal{B}_Q$ divide the respective v and Q planes each into two regions. In the v plane these can be labelled as R_1 and R_2, the exterior and interior of the circle $|v+1| = 1$, and similarly in the Q plane the exterior and interior of the closed curve given by (20). In regions R_1 and R_2 the dominant $\bar{\lambda}$s are $\bar{\lambda}_{\mathrm{sq},1,0}$ and $\bar{\lambda}_{\mathrm{sq},1,1}$, respectively.

For $L_y = 2$, we use the calculation of $Z(\mathrm{sq}[2 \times m], \mathrm{cyc}, Q, v)$ in [4]. From (11) we have $n_Z(2,0) = 2$ and $n_Z(2,1) = 3$, together with $n_Z(2,2) = 1$, for a total of $N_{Z,2,\lambda} = 6$. Specializing to the manifold of (4), we find that

$$\bar{\lambda}_{\mathrm{sq},2,1,1} = 1 + v \tag{21}$$

$$\bar{\lambda}_{\mathrm{sq},2,1,j} = v + 2 \pm \sqrt{2v+3}, \tag{22}$$

where $j = 2, 3$ correspond to $\pm$ and $\bar{\lambda}_{\mathrm{sq},2,0,j}$, given by (16).

For $m \to \infty$, the locus $\mathcal{B}_v$ for this cyclic (or corresponding Möbius) strip, shown in figure 4, is comprised of a single closed curve that intersects the real v axis at $v = 0$ and $v = -\sqrt{2}$ and in a two-fold multiple point at $v = -2$. The image of $\mathcal{B}_v$ in the q plane, $\mathcal{B}_Q$, shown in figure 5, is again a closed curve that crosses the real Q axis once at $Q = 0$ and $Q = 2$ and in a two-fold multiple point at $Q = 4$, separating the complex Q plane into three regions in 1–1 correspondence with those in the v plane. These regions are

- R_1, containing the real intervals $v > 0$ and $v < -2$ and extending outwards to the circle at infinity, and its image in the Q plane, containing the real intervals $Q \geqslant 4$ and $Q \leqslant 0$, in which (with appropriate choice of the branch cut for the square root in (16)) $\bar{\lambda}_{\mathrm{sq},2,0,1}$ is dominant,
- R_2, containing the real interval $-\sqrt{2} \leqslant v \leqslant 0$, and its image in the Q plane containing the real interval $0 \leqslant Q \leqslant 2$, in which $\bar{\lambda}_{\mathrm{sq},2,1,2}$ is dominant,

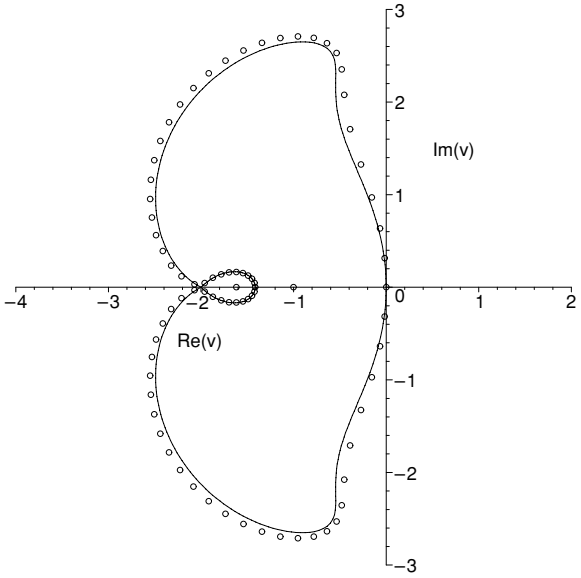

Figure 4. Locus $\mathcal{B}_v$ for the Potts model on a $2 \times \infty$ cyclic or Möbius strip of the square lattice with Q and v satisfying (4). Partition function zeros are shown for a cyclic 2×40 strip.

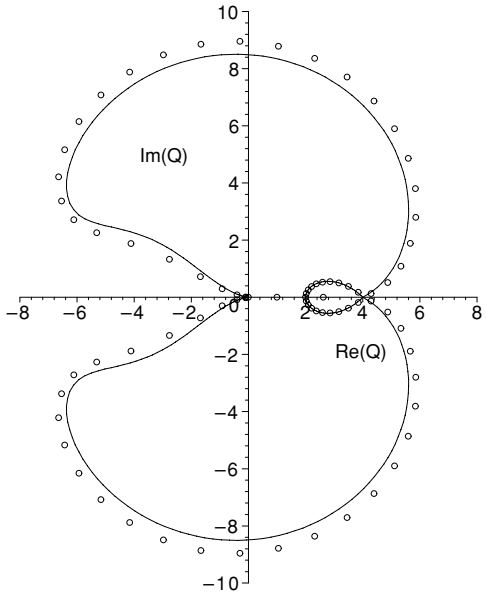

Figure 5. Locus $\mathcal{B}_Q$ for the Potts model on a $2 \times \infty$ cyclic or Möbius strip of the square lattice with Q and v satisfying (4). Partition function zeros are shown for a cyclic 2×40 strip.

- R_3, containing the real interval $-2 \leqslant v \leqslant -\sqrt{2}$ and its image in the Q plane, containing the real interval $2 \leqslant Q \leqslant 4$, in which $\bar{\lambda}_{\mathrm{sq},2,2} = 1$ is dominant.

As was the case for the cyclic $L_y = 1$ strip, the curve $\mathcal{B}_Q$ has a cusp at $Q = 0$. For comparison with the asymptotic loci, in figures 4 and 5 we also show partition function zeros

calculated for a long finite strip, with $m = 40$. One sees that these lie close to the respective loci $\mathcal{B}$.

The exact calculation of $Z(\mathrm{sq}[3 \times m], \mathrm{cyc}, Q, v)$ in [5] has the form of (10) with $L_y = 3$. From (11) we have $n_Z(3, 0) = 5$ and $n_Z(3, 1) = 9$, $n_Z(3, 2) = 5$, together with $n_Z(3, 3) = 1$, for a total of $N_{Z,3,\lambda} = 20$. We specialize to the manifold in (4). Owing to the large number of $\bar{\lambda}_{\mathrm{sq},3,d,j}$ s, we do not list them here. In the $m \to \infty$ limit, we find that $\mathcal{B}_v$ crosses the real v axis at $v = v_2 = 0$, $v = v_4 = -\sqrt{2}$, $v = v_6 = -\sqrt{3}$, and $v = -2$, enclosing several regions in the v plane. The image locus under the map (4), $\mathcal{B}_Q$, crosses the real axis in the interval $0 \leqslant Q \leqslant 4$ at $Q = Q_2 = 0$, $Q = Q_4 = 2$, $Q = Q_6 = 3$, and $Q = 4$. It also crosses the negative real axis at two points corresponding to the two pairs of complex-conjugate points away from $v = 0$ at which $\mathcal{B}_v$ crosses the imaginary axis in the v plane. As with the $L_y = 1$ and $L_y = 2$ cyclic strips, the curves on $\mathcal{B}_Q$ and $\mathcal{B}_v$ separate the respective v and Q planes into several regions in which different $\bar{\lambda}_{\mathrm{sq},3,d,j}$s are dominant.

We have performed corresponding calculations for the cyclic and Möbius strips of the square lattice with $L_y = 4$ and $L_y = 5$. For brevity, we only comment on $\mathcal{B}_Q$ here. We find that $\mathcal{B}_Q$ crosses the real axis in the interval $0 \leqslant Q \leqslant 4$ at $Q = 4$ and at $Q = Q_{2\ell}$ for integer $1 \leqslant \ell \leqslant L_y$ and also on the negative real axis. The outermost complex-conjugate curves on $\mathcal{B}_Q$ continue the trend observed, for smaller widths, of moving farther away from the origin. For example, the outermost curves on $\mathcal{B}_Q$ cross the imaginary Q axis at $Q = \pm 2\mathrm{i}$ for $L_y = 1$, $Q \simeq \pm 8.5\mathrm{i}$ for $L_y = 2$, and at progressively larger values for larger L_y. Similarly, this outermost curve crosses the negative real axis farther away from the origin; the approximate crossing point for $L_y = 3$ is at $Q \simeq -10$, with larger negative values for $L_y = 4, 5$.

3.4. Toroidal and Klein bottle

The exact solution for the partition function on the $L_y = 2$ strip with toroidal boundary conditions which we obtained in [5] has the form of (8) with six λs. Setting $Q = v^2$ (and using the abbreviation sqtor to indicate the boundary conditions), we find

$$\bar{\lambda}_{\mathrm{sqtor},2,j} = \bar{\lambda}_{\mathrm{sqcyl},2,j}, \tag{23}$$

where $\bar{\lambda}_{\mathrm{sqcyl},2,j}$ with $j = 1, 2$ were given above in (17),

$$\bar{\lambda}_{\mathrm{sqtor},2,j} = \tfrac{1}{2}[(v+2)(v+3) \pm [(v^2+3v+8+4\sqrt{2})(v^2+3v+8-4\sqrt{2})]^{1/2}], \tag{24}$$

where $j = 3, 4$ correspond to the $\pm$ signs,

$$\bar{\lambda}_{\mathrm{sqtor},2,5} = v + 1, \tag{25}$$

and

$$\bar{\lambda}_{\mathrm{sqtor},2,6} = 1. \tag{26}$$

In the $m \to \infty$ limit of this strip with toroidal or Klein-bottle boundary conditions, we find that $\mathcal{B}_v$ intersects the real v axis at $v = 0$, $v = -\sqrt{2}$ and $v = -2$. The image curve $\mathcal{B}_Q$, shown in figure 6, thus intersects the real axis at $Q = 0, 2, 4$. These curves divide the respective v and Q planes into three regions. In the v plane, these are (i) the region R_1 including the semi-infinite intervals $v \geqslant 0$ and $v \leqslant -2$ and extending to complex infinity, in which (with appropriate choices of branch cuts for the square roots) $\bar{\lambda}_{\mathrm{sqtor},2,1}$ is dominant, (ii) the region R_2 including the real interval $-\sqrt{2} \leqslant v \leqslant 0$, enclosed by the outer curve, in which $\bar{\lambda}_{\mathrm{sqtor},2,3}$ is dominant and (iii) the region R_3 enclosed by the innermost curve and including the real interval $-2 \leqslant v \leqslant -\sqrt{2}$, in which $\bar{\lambda}_{\mathrm{sqtor},2,6} = 1$ is dominant. Corresponding results hold in the Q plane.

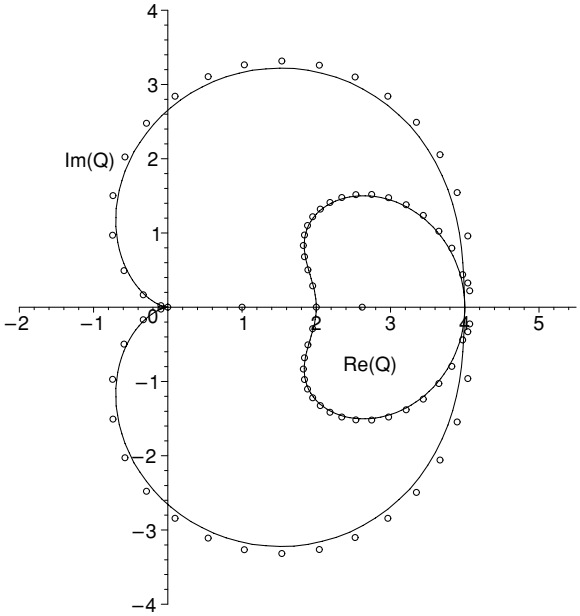

Figure 6. Locus $\mathcal{B}_Q$ for the Potts model on a $2 \times \infty$ strip of the square lattice with toroidal or Klein-bottle boundary conditions and with Q and v satisfying (4). Partition function zeros are shown for a toroidal 2×40 strip.

Using our results in [5, 29], we have also performed similar calculations for the $L_y = 3$ strip of the square lattice with toroidal boundary conditions. We find that $\mathcal{B}_v$ crosses the real axis at $v = 0, v = -\sqrt{2}, v = -2$ and $v \simeq -5.2$ and contains complex-conjugate curves extending to complex infinity in the $\mathrm{Re}(v) < 0$ half plane. Again, corresponding results hold in the Q plane.

4. Strips of the triangular lattice

4.1. General

In order to investigate the lattice dependence of the loci $\mathcal{B}$, we have also calculated these for infinite-length strips of the triangular lattice with various boundary conditions and with Q and v restricted to satisfy the phase transition condition for the two-dimensional triangular lattice, (5). We construct a strip of the triangular lattice by starting with a strip of the square lattice and adding edges connecting the vertices in, say, the upper left to the lower right corners of each square to each other. Since we will find that the values $Q_{2\ell}$ for $\ell = 1, \ldots, L_y$ play an important role for the loci $\mathcal{B}_Q$ for these strips with periodic longitudinal boundary conditions, just as they did for the corresponding square-lattice strips, we give a general solution of (5) for the case where $Q = Q_r$: the roots of this equation are $-1+2\cos(2(r+\eta)\pi)$ with $\eta = 1, -1, 0$, i.e., in order of increasing v,

$$v_{t1}(r) = -1 + 2\cos\left(\frac{2(r+1)\pi}{3r}\right) \tag{27}$$

$$v_{t2}(r) = -1 + 2\cos\left(\frac{2(r-1)\pi}{3r}\right) \tag{28}$$

and

$$v_{t3}(r) = -1 + 2\cos\left(\frac{2\pi}{3r}\right). \tag{29}$$

The relevant case here is $r = 2\ell$ with $1 \leqslant \ell \leqslant L_y$. More generally, for any real $r \geqslant 2$, these roots have the properties

$$v_{t1}(r) \leqslant v_{t2}(r) \leqslant 0 \qquad \text{for} \quad r \geqslant 2 \tag{30}$$

(where the first equality holds only at $r = \infty$ and the second equality holds only at $r = 2$),

$$v_{t3}(r) \geqslant 0 \qquad \text{for} \quad r \geqslant 2 \tag{31}$$

(where the equality holds only at $r = 2$). As r increases from 2 to ∞, (i) $v_{t1}(r)$ increases from -3 to -2, (ii) $v_{t2}(r)$ decreases from 0 to -2 and (iii) $v_{t3}(r)$, which is the physical root for the phase transition on the triangular lattice, increases from 0 to 1.

For the cases of interest here, with $r = 2\ell$ and $1 \leqslant \ell \leqslant L_y$, for widths up to $L_y = 5$, many of the trigonometric expressions in equations (27)–(29) simplify considerably, to algebraic expressions and in some cases to integers, so it is worthwhile displaying these roots explicitly. For $r = 2, 4, 6$, we have

$$\begin{aligned} &v_{t1}(2) = -3, \qquad v_{t2}(2) = 0, \qquad v_{t3}(2) = 0 \quad \Longrightarrow \quad Q = Q_2 = 0 \\ &v_{t1}(4) = -1 - \sqrt{3}, \qquad v_{t2}(4) = -1, \qquad v_{t3}(4) = -1 + \sqrt{3} \end{aligned} \tag{32}$$

$$\Longrightarrow \quad Q = Q_4 = 2 \tag{33}$$

and $v_{tj}(6)$, $j = 1, 2, 3 \quad \Longrightarrow \quad Q = Q_6 = 3$, where

$$v_{t1}(6) = -1 + 2\cos(7\pi/9) \simeq -2.532\,089 \tag{34}$$

$$v_{t2}(6) = -1 + 2\cos(5\pi/9) \simeq -1.347\,296 \tag{35}$$

$$v_{t3}(6) = -1 + 2\cos(\pi/9) \simeq 0.879\,385. \tag{36}$$

For $r = \infty$ we have

$$\begin{aligned} &v_{t1}(\infty) = v_{t2}(\infty) = -2, \qquad v_{t3}(\infty) = 1 \\ &\Longrightarrow \quad Q = Q_\infty = 4. \end{aligned} \tag{37}$$

It is straightforward to work out similar results for other values of r. (Outside of our range, at $r = 1$, since $Q_1 = Q_\infty$, (5) with $Q = Q_1$ has the same set of roots as in (37), with $v_{t1}(1) = v_{t3}(1) = -2$ and $v_{t2}(1) = 1$.) Concerning the behaviour of the solutions of (5) with v as the independent variable, as v decreases from 0, Q increases from 0, reaching a maximum of 4 at $v = -2$ and then decreasing through 0 to negative values as v decreases through -3. Thus, for all v in the interval $-\infty \leqslant v \leqslant 0$, Q is bounded above by the value 4.

4.2. Free strips

The exact solution for the partition function on the $L_y = 2$ strip of the triangular lattice with free boundary conditions in [7] has the form of (8) with two λs. Setting $Q = v^2(v+3)$ as in (5), we find the corresponding reduced $\bar{\lambda}$ s:

$$\bar{\lambda}_{t,2,0,j} = \frac{(v+1)}{2}\left[v^3 + 5v^2 + 9v + 7 \pm (v+3)\sqrt{(v+1)(v^3+3v^2+3v+5)}\right], \tag{38}$$

where $j = 1, 2$ correspond to the $\pm$.

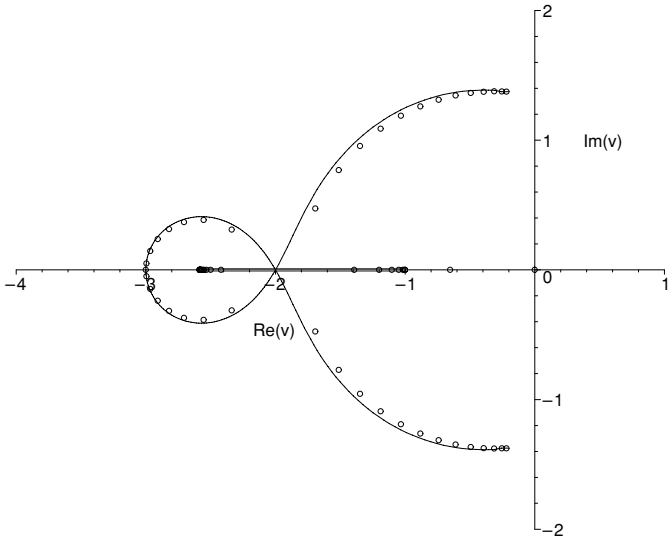

Figure 7. Locus $\mathcal{B}_v$ for the Potts model on a $2 \times \infty$ strip of the triangular lattice with free boundary conditions and with Q and v satisfying (5). Partition function zeros are shown for a free 2×20 strip.

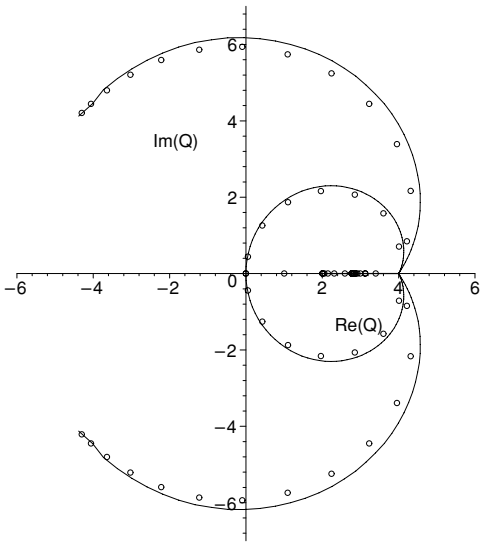

Figure 8. Locus $\mathcal{B}_Q$ for the Potts model on a $2 \times \infty$ strip of the triangular lattice with free boundary conditions and with Q and v satisfying (5). Partition function zeros are shown for a free 2×20 strip.

In the limit $m \to \infty$, we find the locus $\mathcal{B}_v$ shown in figure 7 consisting of the union of (i) a curve that crosses the real v axis at $v = -2$ (a multiple point on the curve) and $v = -3$ and has endpoints at the two complex-conjugate roots of the cubic factor in the square root in (38), $v \simeq -0.206 \pm 1.37\mathrm{i}$ and (ii) a line segment on the real v axis extending from $v = -1$ to $\simeq -2.587$. These endpoints of the line segment are the other two zeros of the polynomial in the square root in (38). This locus divides the complex v plane into two regions. The image of this locus under the mapping (5), $\mathcal{B}_Q$, is shown in figure 8 and consists of the union of a

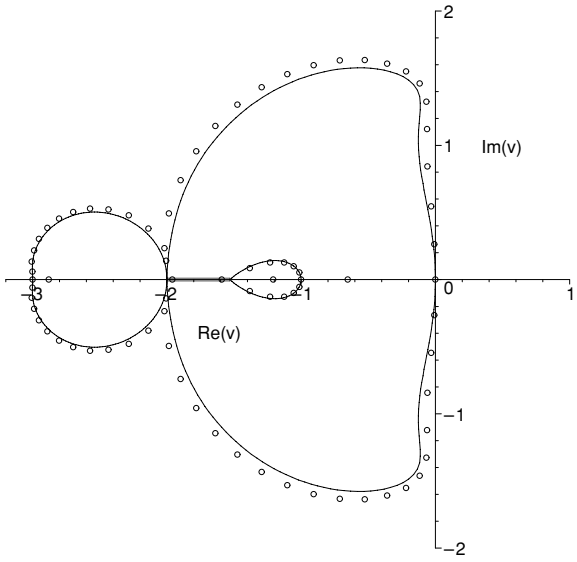

Figure 9. Locus $\mathcal{B}_v$ for the Potts model on a $2 \times \infty$ strip of the triangular lattice with cyclic or Möbius boundary conditions and with Q and v satisfying (5). Partition function zeros are shown for a cyclic 2×20 strip.

closed curve passing through $Q = 0$ and $Q = 4$ with complex-conjugate arcs passing through $Q = 4$ and terminating at endpoints $Q \simeq -4.38 \pm 4.12\mathrm{i}$, and a line segment on the real axis extending from $Q = 2$ to $Q \simeq 2.762$. In figures 7 and 8 we also show zeros calculated for a long finite free $L_y = 2$ strip of the triangular lattice. One sees again that these lie close to the asymptotic loci $\mathcal{B}_v$ and $\mathcal{B}_Q$, as one would expect for a long strip. There are also discrete zeros that do not lie on (or close to) the equimodular curves $\mathcal{B}$. We have already explained the origin of the zero at $(Q, v) = (0, 0)$. In contrast to the situation with free strips of the square lattice, where the zero at $v = 0$ and its image at $Q = 0$ were both isolated, here we find that for the free $L_y = 2$ strip of the triangular lattice (see figures 7 and 8), there is an isolated zero at $v = 0$, but because of the non one-to-one nature of the mapping (5), its image in the Q plane is not isolated but rather is on $\mathcal{B}_Q$. We have also performed analogous studies of wider strips of the triangular lattice using the calculations of [30], and we find qualitatively similar results.

4.3. Cyclic and Möbius strips

For cyclic boundary conditions we have $N_{Z,2,\lambda} = 6, n_Z(2, 0) = 2, n_Z(2, 1) = 3, n_Z(2, 2) = 1$, just as in the square-lattice case. We calculated the general partition function $Z(t[2 \times m], \mathrm{cyc}, Q, v)$ in [7], and this has the form of (10) with $L_y = 2$. Restricting Q and v to satisfy (5), we obtain $\bar{\lambda}_{t,2,2} = 1$, $\bar{\lambda}_{t,2,0,j}$ for $j = 1, 2$ given in (38), and $\bar{\lambda}_{t,2,1,j}$ for $j = 1, 2, 3$, which are solutions to the equation

$$\eta^3 - (v+2)(3v+4)\eta^2 + (v+2)(v+1)(3v^2+9v+4)\eta - (v+1)^2(v^2+3v+1)^2 = 0. \qquad (39)$$

In the limit $m \to \infty$ for this cyclic strip (and for the same strip with Möbius boundary conditions), we find the locus $\mathcal{B}_v$ shown in figure 9 and the corresponding locus $\mathcal{B}_Q$ shown in figure 10. These loci consists of closed curves that intersect the real v and Q axis at the following points, where the value of Q is the image of the value of v under the mapping (5):

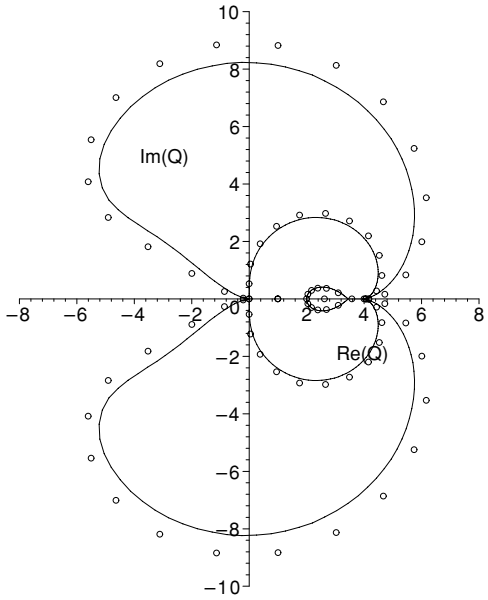

Figure 10. Locus $\mathcal{B}_Q$ for the Potts model on a $2 \times \infty$ strip of the triangular lattice with cyclic or Möbius boundary conditions and with Q and v satisfying (5). Partition function zeros are shown for a cyclic 2×20 strip.

(i) $v = 0$ and $v = -3 \Rightarrow Q = Q_2 = 0$, (ii) $v = -1 \Rightarrow Q = Q_4 = 2$ and (iii) $v = -2 \Rightarrow Q = 4$. The locus $\mathcal{B}_v$ also contains a line segment extending from $v \simeq -1.531$ to $v = -2$, and $\mathcal{B}_Q$ contains its image under the mapping (5) extending from $Q \simeq 3.44$ to $Q = 4$.

The locus $\mathcal{B}_v$ separates the v plane into four regions, as is evident in figure 9:

- the region including the intervals $v \geqslant 0$ and $v \leqslant -3$ on the real v axis and extending to complex infinity, in which (with appropriate definition of the branch cuts associated with the square root in (38)) $\bar{\lambda}_{t,2,0,1}$ is dominant,
- the region including the neighbourhood to the left of $v = 0$ and excluding the interior of the loop centred approximately around $v = -1.2$, in which one of the $\bar{\lambda}_{t,2,1,j}$s is dominant,
- the region in the interior of the loop centred around $v = -1.2$, in which $\bar{\lambda}_{t,2,2} = 1$ is dominant,
- the region including the interval that extends from $v = -2$ to $v = -3$, in which another $\bar{\lambda}_{t,2,1,j}$ is dominant.

We give some specific dominant eigenvalues at special points. At $v = 0$, $\bar{\lambda}_{t,2,0,1} = (7 + 3\sqrt{5})/2$, equal in magnitude to the dominant $\bar{\lambda}_{t,2,1,j}$. At $v = -2$, all of the six $\bar{\lambda}_{t,2,d,j}$s are equal in magnitude and equal to unity. At $v = -3$, $|\bar{\lambda}_{t,2,0,j}| = 2$ for $j = 1, 2$, and two of the $|\bar{\lambda}_{t,2,1,j}| = 2$, while the third is equal in magnitude to 1.

Correspondingly, the locus $\mathcal{B}_Q$ divides the Q plane into five regions:

- the region including the intervals $Q \geqslant 4$ and $Q \leqslant 0$ on the real Q axis and extending to infinity, in which $\bar{\lambda}_{t,2,0,1}$ is dominant,
- two complex-conjugate regions bounded at large Q by curves that cross the imaginary axis at $Q \simeq \pm 8.23\mathrm{i}$, in which one of the $\bar{\lambda}_{t,2,1,j}$s is dominant,

- the region including the interval $0 \leqslant Q \leqslant 2$, in which another $\bar{\lambda}_{t,2,1,j}$ is dominant,
- the region in the interior of the loop centred approximately around $Q = 2.6$, in which $\bar{\lambda}_{t,2,2} = 1$ is dominant.

We have performed similar calculations for cyclic strips of the triangular lattice with greater widths, $L_y = 3, 4, 5$. We find that $\mathcal{B}_v$ crosses the negative real axis at $v_{t2}(2\ell)$ for $1 \leqslant \ell \leqslant L_y$, so that $\mathcal{B}_Q$ crosses the real axis at the image points under (5), $Q_{2\ell}$. As with the cyclic square-lattice strips with widths $L_y \geqslant 3$, we find that the outermost curves on $\mathcal{B}_Q$ cross the negative real axis; for example, for $L_y = 3$, such a crossing occurs at $Q \simeq -9.4$.

4.4. Other strips of the triangular lattice

We have also calculated the partition function and the resultant loci $\mathcal{B}_v$ and $\mathcal{B}_Q$ for strips of the triangular lattice with cylindrical and toroidal boundary conditions. A general feature that we find is that $\mathcal{B}_v$ passes through $v = -2$, and hence $\mathcal{B}_Q$ passes through $Q = 4$. Other features depend on the specific boundary conditions and width. One property that we encounter is noncompactness of $\mathcal{B}_v$ and $\mathcal{B}_Q$ (as was the case with the $L_y = 3$ toroidal strip of the square lattice and for cyclic self-dual strips of the square lattice [15]).

5. Strips of the honeycomb lattice

We first give a general solution for the three roots in v of (6) with $Q = Q_r$; in order of increasing value, these are

$$v_{\rm hc1}(r) = -4\cos\left(\frac{\pi}{r}\right)\cos\left[\frac{\pi}{3}\left(\frac{1}{r} - 1\right)\right] \tag{40}$$

$$v_{\rm hc2}(r) = -4\cos\left(\frac{\pi}{r}\right)\cos\left[\frac{\pi}{3}\left(\frac{1}{r} + 1\right)\right] \tag{41}$$

and

$$v_{\rm hc3}(r) = 4\cos\left(\frac{\pi}{r}\right)\cos\left(\frac{\pi}{3r}\right). \tag{42}$$

As r increases from 2 to ∞ and Q_r thus increases from 0 to 4, (i) $v_{\rm hc1}(r)$ decreases from 0 to a minimum of $-9/4$ at $r = \pi/\arcsin(\sqrt{10}/8) \simeq 7.73$ and then increases to -2; (ii) $v_{\rm hc2}(r)$ decreases monotonically from 0 to -2 and (iii) $v_{\rm hc3}(r)$, the physical root, increases monotonically from 0 to 4. As with the analogous expressions for the triangular lattice, it is straightforward to work out simpler expressions to which equations (40)–(42) reduce for special values of r; we omit the details here.

For this honeycomb lattice, substituting the value $v = -2$ into (6) yields two solutions, $Q = 2$ and $Q = 4$. Using our general solutions for the partition functions $Z(\mathrm{hc}[2 \times m], \mathrm{free}, Q, v)$ and $Z(\mathrm{hc}[2 \times m], \mathrm{cyc}, Q, v)$ in [8], we have checked that at $v = -2$, $Q = 4$ there is degeneracy of dominant λs, so that these points are on the respective loci $\mathcal{B}_v$ and $\mathcal{B}_Q$. This property is thus similar to the feature that we have found for strips of the square and triangular lattices. For $L_y = 2$ cyclic honeycomb-lattice strips we find that, in addition, the points $v = 0$, $Q = Q_2 = 0$ and $v = -2$, $Q = Q_4 = 2$ are on the respective loci $\mathcal{B}_v$ and $\mathcal{B}_Q$. For the $L_y = 3$ cyclic strips of this lattice, $\mathcal{B}_v$ contains these points and also $v_{\rm hc1}(6) = -2\sqrt{3}\cos(5\pi/18)$, so that the image $\mathcal{B}_Q$ contains the point $Q = Q_6 = 3$. For all the strips of this lattice that we have studied, with L_y up to $L_y = 5$, we find that $\mathcal{B}_v$ crosses the real axis at $v = v_{\rm hc1}(2\ell)$ for $\ell = 1, \ldots, L_y$, so that $\mathcal{B}_Q$ crosses the real Q axis at $Q_{2\ell}$ for $\ell = 1, \ldots, L_y$.

6. Discussion and conclusions

In this paper, then, we have presented exact results for the continuous accumulation set $\mathcal{B}$ of the locus of zeros of the Potts model partition function for the infinite-length limits of strips of the square, triangular, and honeycomb lattices with various widths, a variety of boundary conditions, and Q and v restricted to satisfy conditions (4), (5) and (6) for the ferromagnetic phase transition on the corresponding two-dimensional lattices. In this section we give a discussion of, and draw conclusions concerning, several features that are common to all of the strips of the three types of lattices that we have analysed. These include the following:

- For all of the strips, including those of the square, triangular, and honeycomb lattices, that we have studied where nontrivial continuous accumulation loci are defined (thus excluding the $1 \times m$ line graph with free boundary conditions), we find that $\mathcal{B}_v$ passes through $v = -2$ and $\mathcal{B}_Q$ passes through $Q = 4$, which is the image of $v = -2$ under both of the mappings (4) and (5) and is a solution of (6) with $v = -2$.
- For all of the cyclic (and equivalently, Möbius) strips that we have studied, besides the crossing at $Q = 4$, $\mathcal{B}_Q$ crosses the real axis at

$$Q = Q_{2\ell} \qquad \text{for} \quad \ell = 1, \ldots, L_y. \tag{43}$$

  We conjecture that this holds for arbitrarily large L_y. This locus can also cross the real axis at other points, such as the crossings on the negative real axis that we found for widths $L_y \geqslant 3$.

For the particular case of the cyclic square-lattice strips, these properties agree with a result in [25], namely, that at $Q = Q_{2\ell}$, $|\lambda_{\mathrm{sq},L_y,\ell,\max}| = |\lambda_{\mathrm{sq},L_y,\ell-1,\max}|$, where $\lambda_{\mathrm{sq},L_y,\ell,\max}$ denotes the eigenvalue $\lambda_{\mathrm{sq},L_y,\ell,j}$ of largest magnitude.

We also observed that the points $v = -2$ and $Q = 4$ play a special role for self-dual strips of the square lattice in [15]. It is interesting that for self-dual cyclic square-lattice strips, in addition to the point $Q = 4$, $\mathcal{B}_Q$ crosses the real axis at $Q_{2\ell+1}$ for $1 \leqslant \ell \leqslant L_y$. This set of points is interleaved with those in (43). As we have noted in [15], these findings are in accord with the fact that the Potts model at the values $Q = Q_r$ has special properties, such as the feature that the Temperley–Lieb algebra is reducible at these values [24, 25, 31]. A related fact is that complex-temperature phase diagrams of the Potts model show special properties at $Q = Q_r$. (In addition to the trivial cases $Q = Q_2 = 0$ and $Q = Q_3 = 1$ and the exactly solvable Ising case $Q = Q_4 = 2$, complex-temperature phase diagrams have been studied for various Q_r such as $Q_6 = 3$ and $Q_1 = Q_\infty = 4$ [3–5, 7, 8, 27–30] and [32–39]). In [15] we compared our exact results for $\mathcal{B}$ on infinite-length, finite-width cyclic self-dual strips of the square lattice with calculations of partition function zeros for finite $L \times L$ sections of the square lattice with $Q = v^2$ in [40] with the same boundary conditions. For finite lattice sections, there is, of course, no locus $\mathcal{B}_Q$ defined, and hence one is only able to make a rough comparison of patterns of zeros. In the calculation of zeros for the above-mentioned $L \times L$ section of the square lattice with cyclic self-dual boundary conditions, e.g., for $L = 8$, a number of zeros in the Q plane occur at or near to certain Q_r s, and the zeros in the v and Q planes exhibit patterns suggesting the importance of the points $v = -2$ and $Q = 4$. With our results in the present paper, we can extend this comparison. We see that the importance of $v = -2$ and $Q = 4$ for the pattern of partition function zeros for Q and v satisfying relation (4) generalizes to square-lattice strips with a variety of boundary conditions, not necessarily self-dual. Indeed, going further, our results show that the features we have observed are true not just of the partition function on the square-lattice strips with $Q = v^2$, but also on strips of the triangular and honeycomb lattices with Q and v satisfying the analogous phase transition conditions (5) and (6).

One interesting aspect of the findings in the present work and our paper [15] on infinite-length, finite-width strips is the special role of the value $Q = 4$ for the loci $\mathcal{B}_Q$, which can make a connection with the locus $\mathcal{B}$ for the physical phase transition of the Potts model on two-dimensional lattices. In this context, we recall that the value $Q = 4$ is the boundary between the interval $0 \leqslant Q \leqslant 4$ where the paramagnetic to ferromagnetic phase transition of the 2D Potts model is continuous (second order) and the interval $Q > 4$ where it is first order. Although the Potts model (and more generally any spin model with finite-range spin–spin interactions) has no finite-temperature phase transition on these quasi-one-dimensional strips, it is, nevertheless, intriguing that if one restricts Q and v to satisfy the conditions corresponding to the ferromagnetic phase transition on a square, triangular, or honeycomb lattice, then the value $Q = 4$ plays a special role not only for the nature of the transition and associated singularities on the infinite 2D lattice, but also for the singular locus $\mathcal{B}$ for infinite-length, finite-width strips.

Acknowledgments

This research was partially supported by the Taiwan NSC grant NSC-94-2112-M-006-013 (S-C C) and the US NSF grant PHY-00-98527 (RS).

References

[1] Wu F Y 1982 *Rev. Mod. Phys.* **54** 235
[2] Baxter R J 1982 *Exactly Solved Models in Statistical Mechanics* (New York: Academic)
[3] Martin P 1991 *Potts Models and Related Problems in Statistical Mechanics* (Singapore: World Scientific)
[4] Shrock R 2000 *Physica* A **283** 388
[5] Chang S C and Shrock R 2001 *Physica* A **296** 234
[6] Fisher M E 1965 *Lectures in Theoretical Physics* vol 7C (Boulder, CO: University of Colorado Press) p 1
[7] Chang S C and Shrock R 2000 *Physica* A **286** 189
[8] Chang S C and Shrock R 2001 *Physica* A **296** 183
[9] Abe R, Dotera T and Ogawa T 1991 *Prog. Theor. Phys.* **85** 509
[10] Matveev V and Shrock R 1996 *J. Phys. A: Math. Gen.* **29** 803
[11] Shrock R and Tsai S H 1997 *Phys. Rev.* E **55** 5165
[12] Chang S C and Shrock R 2001 *Physica* A **301** 301
[13] Lieb E H 1967 *Phys. Rev.* **162** 162
[14] Biggs N and Shrock R 1999 *J. Phys. A: Math. Gen.* **32** L489
[15] Chang S C and Shrock R 2006 *Preprint* cond-mat/0602178
[16] Kasteleyn P and Fortuin C 1969 *J. Phys. Soc. Japan. Suppl.* **26** 11
[17] Fortuin C and Kasteleyn P 1972 *Physica* **57** 536
[18] Biggs N 1993 *Algebraic Graph Theory* (Cambridge: Cambridge University Press)
[19] Tutte W T 1967 *J. Comb. Theory* **2** 301
[20] Tutte W T 1970 *J. Comb. Theory* **9** 289
[21] Tutte W T 1974 Chromials, *Lecture Notes in Mathematics* vol 411, p 243
[22] Beraha S, Kahane J and Weiss N 1979 *J. Comb. Theory* B **27** 1
[23] Beraha S, Kahane J and Weiss N 1980 *J. Comb. Theory* B **28** 52
[24] Saleur H 1990 *Commun. Math. Phys.* **132** 657
[25] Saleur H 1991 *Nucl. Phys.* B **360** 219
[26] Chang S C and Shrock R 2001 *Physica* A **296** 131
[27] Chang S C, Salas J and Shrock R 2002 *J. Stat. Phys.* **107** 1207
[28] Chang S C and Shrock R 2005 *Physica* A **347** 314
[29] Chang S C and Shrock R 2006 *Physica* A **364** 231
[30] Chang S C, Jacobsen J, Salas J and Shrock R 2004 *J. Stat. Phys.* **114** 763
[31] Martin P 1987 *J. Phys. A: Math. Gen.* **20** L399
[32] Martin P and Maillard J M 1986 *J. Phys. A: Math. Gen.* **19** L547
[33] Chen C N, Hu C K and Wu F Y 1996 *Phys. Rev. Lett.* **76** 169

[34] Matveev V and Shrock R 1996 *Phys. Rev.* E **54** 6174
[35] Feldmann H, Shrock R and Tsai S H 1997 *J. Phys. A: Math. Gen.* **30** L663
[36] Feldmann H, Shrock R and Tsai S H 1998 *Phys. Rev.* E **57** 1335
[37] Feldmann H, Guttmann A J, Jensen I, Shrock R and Tsai S H 1998 *J. Phys. A: Math. Gen.* **31** 2287
[38] Chang S C and Shrock R 2001 *Phys. Rev.* E **64** 066116
[39] Jacobsen J, Richard J F and Salas J 2006 *Nucl. Phys.* B **743** 153
[40] Kim S Y and Creswick R 2001 *Phys. Rev.* E **63** 066107